Active retinal tracker for clinical optical coherence tomography systems

Daniel X. Hammer
R. Daniel Ferguson
John C. Magill
Physical Sciences Inc.
20 New England Business Center
Andover, Massachusetts 01810
E-mail: hammer@psicorp.com

Lelia Adelina Paunescu
Siobahn Beaton[†]
Hiroshi Ishikawa[†]
Gadi Wollstein[†]
Joel S. Schuman[†]
New England Eye Center
New England Medical Center
750 Washington Street, Box 450
Boston, Massachusetts 02111

Abstract. An active, hardware-based retinal tracker is integrated with a clinical optical coherence tomography (OCT) system to investigate the effects of stabilization on acquisition of high-resolution retinal sections. The prototype retinal tracker locks onto common fundus features, detects transverse eye motion via changes in feature reflectance, and positions the OCT diagnostic beam to fixed coordinates on the retina with mirrors driven by a feedback control loop. The system is tested in a full clinical protocol on subjects with normal and glaucomatous eyes. Experimental analysis software is developed to coalign and coadd multiple fundus and OCT images and to extract quantitative information on the location of structures in the images. Tracking is highly accurate and reproducible on all but one subject, resulting in the ability to scan the same retinal location continually over long periods of time. The results show qualitative improvement in 97% of coadded OCT scans and a reduction in the variance of the position of the optic disc cup edge to less than 1 pixel (<60 μm). The tracking system can be easily configured for use in research on ultra-high-resolution OCT systems for advanced image modalities. For example, tracking will enable very high density 3-D scans of the retina, which are susceptible to eye motion artifacts even for new high-speed systems.
[DOI: 10.1117/1.1896967]

Keywords: retinal tracker; image stabilization; optical coherence tomography; glaucoma; retina; low-coherence imaging.

Paper 03151 received Dec. 18, 2003; revised manuscript received May 25, 2004; accepted for publication Sep. 9, 2004; published online Apr. 13, 2005.

1 Introduction

Optical coherence tomography (OCT) has rapidly become a standard clinical tool for ophthalmologist in the diagnosis of retinal diseases.[1] OCT uses heterodyne detection of backscattered low-coherence light scanned transversely and axially to produce high-resolution 2-D sections of tissues. In the eye, OCT has been used to image macular edema,[2] macular holes, retinal detachments,[3] and retinal vein occlusions[4] among other conditions. One of the most promising applications of OCT in ophthalmic imaging is for the early diagnosis of glaucoma.[5] This application requires accurate and reproducible measurement of retinal nerve fiber layer (RNFL) for multiple patient visits over an extended period of time. Clinical OCT instruments have been shown[6] to produce highly accurate maps of RNFL.

Although the image orientation for OCT differs from other types of retinal diagnostic techniques such as flash fundus photography and scanning laser ophthalmoscopy (SLO), OCT is limited by the same physical parameters as other imaging types. For example, OCT and SLO both use focused coherent light and are therefore restricted by ANSI standards to certain radiant exposure levels delivered to the eye. To collect photons at a sufficient SNR to produce high-quality images, the frame rate must be kept low.[7] Another limitation in retinal imaging is imposed by involuntary eye motion (e.g., microsaccades), which conversely requires very rapid frame rates to produce sharp images. Even in patients that are good fixators, eye motion amplitude may be several hundred micrometers, much larger than the transverse resolution of the recently released third-generation Carl Zeiss Meditec, Inc. (CZMI) OCT instrument (Stratus OCT). Also, patients with diseases such as glaucoma require image registration over long periods of time (i.e., years) to accurately track disease progression. Moreover, advanced imaging modalities, such as full 3-D maps of the retina, are susceptible to eye motion artifacts because of the duration of the scan (even for spectral domain OCT). OCT is therefore ideally suited for application of a retinal tracking technique.

We modified and tested a commercial clinical OCT system to include an active, hardware-based retinal tracker for image stabilization. The new experimental instrument, called tracking optical coherence tomography (TOCT), uses a laser beam dithered on common fundus features and phase sensitive detection to track eye motion.[8] This type of retinal tracker is distinguished from other eye trackers in both target and speed.

[†]Current Address: University of Pittsburgh School of Medicine, The Eye and Ear Institute, Suite 816, 203 Lothrop Street. Pittsburgh, Pennsylvania 15213.

1083-3668/2005/$22.00 © 2005 SPIE

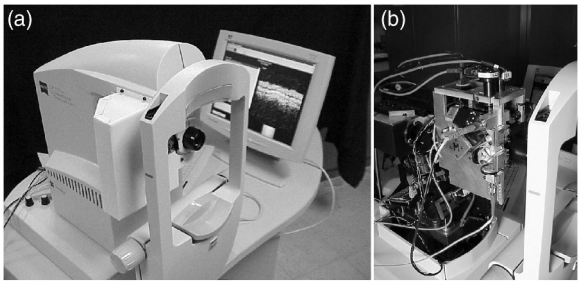

Fig. 1 Photograph of TOCT system: (a) clinical prototype (tracking optics enclosed on left) and (b) with tracking optics exposed.

Most eye trackers target the anterior segment, such as those active trackers that use Purkinje reflections from the cornea. To register frames, other eye trackers use a passive software-based image processing approach, limited by camera frame rate. The retinal tracking system operates with a closed-loop bandwidth in excess of 1 kHz, which thereby renders OCT scans insensitive to all rotational (but not torsional) eye motion. This paper describes the TOCT, clinical trials to characterize tracking improvement, and software developed to analyze clinical results.

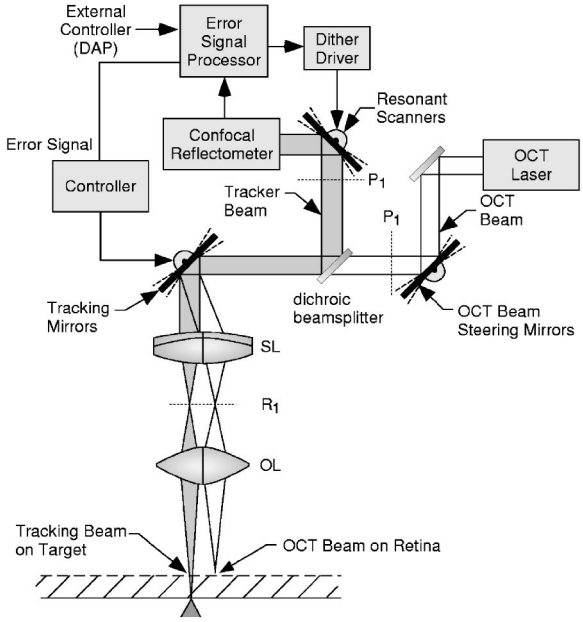

Fig. 2 Tracking portion of TOCT system: SL, scan lens; OL, opthalmoscopic lens; R_1, retinal conjugate; and P_1, pupil conjugate.

2 TOCT System Overview

The experimental TOCT is comprised of a hardware-based, active retinal tracker incorporated into a clinical OCT II instrument, manufactured by CZMI. A picture of the optical head of the TOCT instrument is shown in Fig. 1. The retinal tracking software user interface, written in LabVIEW (National Instruments Inc.), was run on a separate computer from the OCT system. The computer also housed a real-time digital acquisition processor (DAP, Microstar Laboratories Inc.) and an analog framegrabber (National Instruments Inc.). Several instrumentation boxes contained detection, signal processing, and power supply electronics for the retinal tracker.

Figure 2 is an illustration of the tracking portion of the TOCT system. A complete description of the principle of operation of the retinal tracker can be found elsewhere.[9,10] The retinal tracking system consists of a confocal reflectometer, a pair of resonant scanners, and a pair of galvanometer-driven tracking mirrors. The OCT scan is produced with a second pair of galvanometer-driven mirrors. The tracking beam is dithered on a retinal target with the resonant scanners and the reflectance signal from that target is used to control the position of tracking mirrors, through which both the tracking and OCT beams pass. The pupil of the eye is imaged between the two dither scanner mirrors. The tracking and OCT beams are combined by transmission through and reflection off a dichroic beamsplitter. This arrangement, which requires no less than 20 nm of separation between the edge (FWHM) of the near-IR OCT spectrum (centered at 820 nm with a bandwidth of 25 nm) and tracking beam wavelength (860 nm) and the sharpest possible filter cut-on at 850 nm, eliminates the necessity for reimaging of the tracking beam. The result is the ability to aim the OCT beam and tracking beam independently of each other. The tracking mirrors were placed as close as possible to the conjugate to the center of rotation of the eye. This placement provides simultaneous partial pupil tracking for the maximum tracking range without vignetting by the pupil and maintains nearly equal angular magnification for the x and y tracking mirrors.

Due to the high longitudinal magnification of the scanning optics path, the scanning mirrors were placed very close together at the eye pupil plane conjugate. This design provides a fairly simple and reliable interface to the eye, with an ophthalmoscopic objective that provides the required field of view (~30 deg) at the retina. The placement of the OCT scanning mirrors and dither scanners very near the pupillary conjugate ensures that OCT and tracking beams will pass through the cornea at the full scan angle range without vignetting by the pupil.

The fundus viewing path of the OCT II uses another dichroic beamsplitter to separate the visible illumination wavelengths (<800 nm) from the OCT band. The coating of the fundus viewing beamsplitter was designed for efficient reflection of the OCT beam. Since the tracking beam must also be efficiently turned by this beamsplitter, a 2-mW (typically ~25 μW at the cornea), narrowband 860-nm vertical-cavity surface-emitting (VCSEL) laser diode (Lasermate Corp.) was used to fulfill the beam wavelength separation requirement of the first dichroic beamsplitter. The transmit and receive ports of the tracker reflectometer were coupled to the VCSEL source and an avalanche photodiode detector (Hamamatsu Inc.) via multimode fibers with a range of core sizes to control tracking beam size. A 100-μm-diam core fiber was used in the clinical trials for tracking on the optic nerve head, which produced a ~350-μm beam diameter at the retina. Smaller fibers that produce a smaller tracker beam diameter may be more appropriate for tracking other retinal targets such as blood vessel junctions. To eliminate possible tracking interference from the OCT beam itself, an 860-nm, 10-nm FWHM bandpass filter was used in front of the detector.

Table 1 Scan type (corresponding to Fig. 3) and number for each subject visit in the clinical protocol.

Figure	Trials	n^a	Scan Type	Pixel (μm)	Target	N^b
3(a)	1	20	Circle	109	Optic disc	40
3(b)	3	6	Radial	59	Optic disc	36
3(c)	3	6	Radial	59	Fovea	36
Total						112

[a] Number of scans in each set.

[b] Total number of scans in all sets (tracking and nontracking).

Although the optical paths of the OCT and retinal tracker instruments were combined, the software and user interface for both systems remained essentially independent of one another. CZMI software controlled, acquired, and displayed the OCT scans. The retinal tracker control software and user interface were similar to other implementations of retinal tracking.[9–11] The TOCT functioned quite robustly even though the two systems were functionally independent.

3 Clinical Trial Protocol and Procedure

The clinical protocol called for a series of OCT scans to be collected both with and without the retinal tracker engaged on three visits to the clinic. Two groups of subjects were recruited, one with normal, healthy eyes and one with glaucomatous eyes. The normal subjects were recruited from New England Medical Center (NEMC) and Physical Sciences Inc. staff. The glaucoma subjects were recruited from the patient population of NEMC. All subjects gave written informed consent, which was approved by the NEMC Institutional Review Board (IRB) prior to the study. The tracking feature for all scans was the lamina cribrosa, a bright layer within the optic nerve head. The lamina cribrosa is generally a stable, robust feature with characteristics suitable for tracking. The sequence of OCT scans used in this protocol for each visit is listed in Table 1. For each type of scan, the order of scans acquired with and without tracking was randomized. Figure 3 illustrates the scan types listed in Table 1. The scan length (circumference) of the peripapillary scan [Fig. 3(a)] is 10.85 mm, corresponding to a nominal angular diameter of 12 deg and a nominal transverse resolution of 108.5 μm (100 pixels). The peripapillary scan is generally used to measure retinal nerve fiber layer (RNFL) thickness around the optic disc to screen for or monitor subjects with glaucoma. The radial scan set consists of six scans successively rotated by 30 deg and centered either on the optic disc or the fovea [Figs. 3(b) and 3(c)]. The scan length of the radial scan is 5.9 mm or 20 deg and the nominal transverse resolution is 59 μm. The radial scan is used to generate a map of a large region of the macula or disc for measurement of RNFL or retinal thickness or disc parameters (disc rim, disc area, cup area, etc).

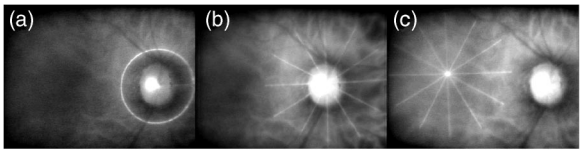

Fig. 3 Fundus images illustrating OCT scan types used in this clinical trial: (a) peripapillary scan (single fundus image), (b) disc radial scan, and (c) fovea radial scan. Fundus images of radial scans were created by coadding six individual images while the tracker was engaged (normal subject 10, OD).

A total of 11 subjects with normal healthy eyes and 11 subjects with glaucomatous eyes were scanned in the full protocol. Glaucomatous eyes had visual field glaucoma hemifield test outside normal limits and/or nerve fiber layer defect on stereo biomicroscopy. For all subjects, refractive error was between -7.0 and $+3.0$ diopters and best-corrected visual acuity was 20/40 or better. Two subjects had intraocular lenses (IOL) and one subject had a grade 1 cataract. Women comprised 45% and minorities (Asian American and African American) comprised 14% of the study group. The median age (range) for the normal group was 39 (26 to 58) and for the glaucoma group was 70 (42 to 85). In addition, two normal subjects partially completed the full protocol (single complete visits) and four more were scanned to test tracking fidelity. Of the 28 scanned, only 1 was disqualified from participation due to a condition that affected tracking. This condition, known as spontaneous venous pulsation, which causes vessels within the optic nerve head to collapse when the intraocular pressure exceeds the venous pressure during the cardiac cycle, caused a modulation in the reflectance with heart rate from the vessel that lay over the lamina cribrosa. Although this modulation did not prevent the system from tracking, the tracking position shifted during the cardiac cycle. Three glaucoma subjects also exhibited multiple tracking loci within the lamina cribrosa. Although tracking was robust on individual loci, this characteristic of lamina cribrosa for a fraction of patients led to errors when tracking was initiated on different loci within the same scan set. Subjects with multiple tracking loci were included in the analysis despite the occurrence of operator errors.

4 Analysis Methods

The goal of the clinical protocol was to measure, both qualitatively and quantitatively, the transverse image registration achieved by TOCT compared to that achieved by the unaided subject who is asked to fixate. The amplitude of involuntary microsaccades for a good fixator is approximately 0.3 deg. If drift and other types of fixational eye motion are also considered, a reasonable estimate for the amplitude of eye motion while a healthy subject fixates is $\sim$0.5 deg ($\sim$150 μm). For peripapillary and radial OCT scans, respectively, this corresponds to approximately 1.4 and 2.5 transverse pixels. Since reproducibility in scan-to-scan registration is the ultimate measure of success, the appearance and position variance of landmarks in coadded images was the primary analysis endpoint. Image coaddition is defined in this paper as the additive accumulation of a set of aligned OCT or fundus images. Averaging is generally used to increase SNR, since decorrelated noise varies inversely with the square root of the number of measurements. Speckle is not random noise, nor is it determined by an intrinsic reflectance property of tissue. From the standpoint of imaging, it can be regarded as an image noise source. Speckle in OCT images of biological tissue, which arises from interference of the fraction of cellular constituents

that are in relative motion, should be reduced by up to the square root of the number of measurements. Comparison of qualitative improvement in coadded OCT images can be accomplished by observation of the sharpness of fine structures and layers within the retina. One type of fine structure that is readily apparent in the coadded cross-sectional images is blood vessels, which leave a shadow in the regions below them due to the relatively high extinction by blood at these wavelengths.

Although the accuracy of the tracking system was found to be <0.05 deg (~ 15 μm) in other implementations of retinal tracking[9] (TSLO), the analysis of OCT images from this protocol is not expected to yield similar results because the transverse scan resolution for the OCT II platform is much larger. The tracking accuracy measured from OCT scans will therefore scale with transverse image resolution until the image resolution is better than the ultimate noise-limited performance of the tracking system.

The analysis software built into the OCT system provides quantitative information on retinal and RNFL thickness, but does not include a suitable algorithm to measure the improvement due to retinal tracking. Because the gradients of the horizontal retinal layers are shallow, even in subjects with glaucoma, thickness measurement of these layers is less sensitive to motion than retinal structures with small transverse dimensions (e.g., blood vessels). Thus, the appearance of some features of the coadded scans for tracking and nontracking is quite similar because the layer thickness does not change rapidly in the retinal plane. Therefore, we developed a library of software routines (with simple graphical user interfaces, GUIs) in LabVIEW g-programming language (National Instruments Inc.) specifically designed to automate the process by which qualitative and quantitative measures of the improvement due to tracking are collected from the large data set of each subject. The software includes the following overall functions: (1) an alignment algorithm was written to register and coadd fundus images for an en face view of the retinal region scanned; (2) a *z* axis alignment algorithm created for use on all sets of OCT scans to be registered and coadded; and (3) an edge position measurement algorithm, created to provide a measure of the variance of the position of a landmark edge in a set of individual scans. These functions are discussed in detail in the following sections. In addition to these algorithms, the software library included functionality to read, write, and resize OCT and fundus images, stretch and equalize all images, sort and display OCT and fundus images within various data sets, remove poor quality images or those collected in error, set analysis parameters from dialog boxes from the GUI front panel, and save analysis data.

4.1 *Fundus Image Registration Software*

For each OCT scan collected, a fundus image is also saved. Since the design of the OCT II instrument was optimized for retinal cross-sectional rather than direct fundus (en-face) imaging, the quality of the fundus images is not intended to be as good as other types of ophthalmic imaging technologies (i.e., SLO). However, the fundus images show sufficiently good detail of retinal features to provide useful qualitative information on tracking accuracy and reproducibility. Therefore, a software program was devised and developed to coalign sets of fundus images. The software algorithm works by registration of all fundus images in a set to the position of the OCT beam. If the eye moves with respect to the OCT scan, features will appear blurry in the coadded fundus image. If the eye is made stationary with respect to the OCT scan, fundus features will appear sharp.

For both peripapillary and radial scans, the algorithm precisely locates the center of the OCT scan in the single fundus images, translates each image to align the OCT scan center to a common point, and coadds all of the images in a set. The accuracy of the algorithm can be seen by comparison of the sharpness of the OCT beam in the coadded fundus image to the sharpness in a single fundus image. In other words, if there is any blur in the OCT beam (or in the worse case scenario, multiple OCT beams), then it is clear that the algorithm failed. However, the sharpness of the OCT beam did vary from person to person because of the variance in fundus reflectivity, because many subjects had poor ocular optics that did not allow clear visualization of the fundus, and because the OCT beam was often inadvertently not correctly focused.

4.2 *OCT Scan Registration Software*

Commercial OCT analysis software generally contains an algorithm for *z* axis registration. This algorithm is able to remove depth motion since OCT scans are, by design, acquired with high depth resolution such that the fast scan axis is the *z* axis (10-ms total depth scan duration). Therefore, the time duration between adjacent transverse pixels is longer than for other video rate en-face imaging techniques (e.g., SLO). SLO instruments, with an image duration of 33 ms but an extremely long confocal range gate in the eye, are susceptible to transverse motion since depth information is essentially unresolved. Conversely, OCT instruments have extremely high depth resolution (i.e., 8 to 15 μm for OCT II). Depth motion is uncompensated by the transverse tracking system and must be corrected in all the OCT images. Although the OCT II alignment software corrects for depth motion in single OCT images, alternate scan alignment software was developed to coalign multiple sets of OCT images.

The *z* axis alignment algorithm was developed to align a weighted mean contour estimate to preserve real surface height information to the extent possible. This algorithm locates a feature or layer in every depth scan and aligns to the same *z* location all the depth scans from a set of OCT images to be coadded. The layers are located by different edge detection algorithms. The edge detection algorithms were required to work equally well for every depth scan through different portions of the retina. For radial scans through the disc, the retinal or optic disc edge is easily located simply by finding the first pixel above a threshold as the pixel index (i.e., location in depth) is increased. Since the vitreous is transparent, there is a large sharp increase in pixel intensity at the inner limiting membrane (i.e., vitreoretinal interface, the inner limiting membrane is not resolved with OCT). A median filter is applied to the retinal edge to remove any errors that arise from spurious signals or pixel noise. The median filter rank is kept as small as possible (default rank=3) to preserve edges and depth motion (subsequently corrected for). This simple method was extremely robust—very few errors inherent to the algorithm (choice of threshold or median filter rank) resulted during analysis of hundreds of OCT images (and thousands of depth scans) from the study group even though the same pa-

rameters were used for every patient. False edges were rare because the OCT reflectance gradient at the inner limiting membrane, which depended to a large extent upon the fixed OCT beam power, was fairly constant.

For radial scans through the fovea, the described threshold algorithm is inappropriate because at the fovea, the OCT signal is often extremely weak and thus the retinal edge not easily located. Therefore an algorithm was developed to locate the strongly backscattering retinal pigment epithelium (RPE) edge. The target edge here is between the photoreceptors, which have extremely low pixel intensity, and the second major bright layer in the OCT image caused by the RPE and highly vascular choriocapillaris. Since the thickness and brightness of every individual's anterior retinal layers (RNFL to the photoreceptors) is variable, the region to threshold is unknown. However, since this region has the largest gradient, standard edge detection and correlation algorithms used for image processing can be employed. The algorithm implemented first applies a median filter to every depth scan, takes the derivative to locate sharp gradients, and uses a peak detection algorithm to find the two largest gradients. The rank of the median filter can be made large to minimize false peaks (default rank=7), as the rank will have only minimal effect over the location of the final peak. Absent excessive noise, the derivative peaks result from the inner limiting membrane and the RPE/choriocapillaris where the change in pixel intensity is largest. The second peak is the target for this algorithm. Finally, a median filter with low rank (default rank=3) is applied to remove any errors in the edge/peak detection algorithms. This algorithm was also very robust with very few errors in the hundreds of OCT images analyzed.

Although the second algorithm worked well for radial scans through the fovea, it will not work for radial scans through the disc since there is no second edge corresponding to the RPE. Therefore, two different edge detection algorithms were necessary. The edge detection algorithms also performed better than other types of correlation algorithms. For the peripapillary scans, both algorithms worked reasonable well. In general, the retinal edge algorithm worked better, although for subjects with a thin RNFL thickness in this scan region (i.e., glaucoma patients), the RPE edge algorithm frequently worked better.

The next step is to align multiple OCT images so that they can be coadded. After the edge (retinal or RPE) of each OCT image is located, a weighting factor w is calculated. This factor is derived from the fact that depth motion is proportional to the total length of an edge or interface (e.g., inner limiting membrane). Therefore, the weight was calculated as the inverse of the total edge length (mean-squared distance calculation). For a set of n OCT images, the mean shift μ, as a function of transverse position x, is then calculated from

$$\mu(x) = \frac{\Sigma_{i=0}^{n} w_i L_i(x)}{\Sigma_{i=0}^{n} w_i},$$

where L is the depth of the retinal or RPE edge as a function of transverse position. Thus, every depth scan in the set of OCT images is shifted to a location that corresponds to the weighted mean of the set. In principle, by using a weighted mean of the location of the edge for several individual scans, motion artifacts can be removed while anatomical contours are maintained. In practice, some small amount of residual depth motion could remain in the OCT image, particularly if the number of images coadded was small. Once the depth scans are shifted, the OCT images are coadded.

The final step in the OCT scan registration software is to flatten the final coadded OCT image. The procedure shifted the RPE edge in each depth scan of the coadded OCT image to a fixed position. Flattening the RPE edge rather than the retinal edge preserves topographical information of the retinal surface. This last step is optional for the peripapillary and fovea radial scans (it may aid in visualization of some structures within the retina but may distort the actual retinal curvature) but was not used for the disc radial scans, because the disc lacks an RPE layer.

4.3 *Edge Position Measurement Software*

The analysis algorithms in the preceding sections will result in the creation of coadded OCT images for qualitative comparison. To establish a quantitative measure of tracking accuracy and reproducibility, the variance of the location of image landmarks with sharp gradients must be measured. In the radial disc scans, the edge of the disc is a clear and appropriate landmark. In the macular radial scans, the foveal pit is also a potential landmark. However, as already discussed, the bottom edge of the foveal pit is difficult to locate since it is absent the overlying layers (RNFL to outer nuclear layer) of the peripheral retina and the photoreceptors have extremely weak back-reflectance. In the circular disc scan, there are no clear landmarks to measure transverse position variance. In all scans, blood vessel shadows are potential markers but may not have sufficient contrast in the individual OCT images to compare. In general, the retinal and choroidal layers do not have a sharp enough gradient to make a meaningful measurement. Because of these difficulties, we report only on measurements made on the relative location of the edge of the optic nerve head acquired with radial OCT scans. Future analysis may focus on extraction of quantitative information from the other types of scans.

After retinal edge detection but prior to depth scan registration, the full width half maximum (FWHM) of both the right and left edges was found. The algorithm finds the baseline, the maximum, and the index that corresponds to the FWHM point. It was important to perform the measurement prior to alignment as the reregistration process could mask transverse motion if there were spikes in the shift of individual scans because of movement of the edges. Thus, the analysis was performed on essentially raw data and unfortunately was susceptible to errors caused by depth motion. It was also important to include both edges of the optic nerve head. Since eye movement is possible in every transverse direction, the vector component of motion normal to the OCT scan plane will cause out-of-plane errors and a change in the area of the optic disc cup during saccades. Therefore, the measured left and right edges of the disc cup may shift by different amounts for a nonsymmetrical cup.

To facilitate accurate measurement of baseline and hence disc cup edge, a flattening algorithm was implemented (different from the final flattening of the coadded OCT images described in Sec. 4.2). The algorithm measures the slope of the left and right baseline regions that do not include the disc

cup (i.e., usually omitting the central 40 pixels), and shifts the scan (in the opposite direction) by the pixel value calculated from the slope. Since the region where the optic nerve head is located is omitted, no artifact is introduced to the edge location from the flattening. The software was written to ensure that no discontinuities were introduced in the retinal edge from the flattening. In addition to the disc cup edges, the disc cup and foveal pit area were also measured by the software using discrete integration.

5 Results

5.1 *Peripapillary Scans*

The average fundus images with and without tracking for each visit of each subject were compared after application of the registration software detailed in Sec. 4.1. For two subjects with poor ocular transmissivity (three visits), the OCT scan was not intense enough or the quality of the fundus images did not support registration. Approximately 20 images were coadded to produce the final average fundus image for the peripapillary scan type. A qualitative improvement (sharpness of edges along vessels and the optics disc) was found in 94 and 82% of the total visits for normal and glaucoma subjects, respectively. Of the visits where no improvement was seen, evaluation of the original fundus images suggested that focus and alignment were not properly optimized, resulting in a lack of sharp edges and insufficient fundus illumination because of vignetting by the pupil. Therefore, the averaged fundus images do not give a final measure of tracking improvement but merely indicate those fundus images where clear improvement occurred.

The average OCT peripapillary scans were similarly compared after application of the registration and coaddition software detailed in Sec. 4.2. For the OCT images, the qualitative criteria for improvement due to eye motion stabilization were the number and width of blood vessel shadow edges, and the clarity of clearly identifiable features such as distinct retinal and subretinal layers. For example, the most posterior layer visible in OCT images is the choriocapillaris due to decreased signal caused by absorption and scattering from overlying structures. The degree to which these structures (vessels, etc.) can be visualized within this layer depends on the ability to stabilize eye motion. Improvement in OCT images taken with tracking compared to without tracking was found in 100 and 94% of the total visits for normal and glaucoma subjects, respectively. Figures 4 and 5 present representative results from one normal and one glaucoma subject. Note the significant reduction of speckle in the averaged OCT images [Figs. 4(b) and 4(c) and 5(b) and 5(c)]. The measured image SNR for the coadded OCT images in Figs. 4 and 5 is 2.8 and 3.5 times greater than the single OCT images from the same set, respectively. The increase in SNR was nearly the same for tracking and nontracking sets. This implies that the large degree of speckle decorrelation between scans (over many seconds at least) is an intrinsic property of the OCT signal in each voxel. Also note the blurred retinal features in the coadded fundus images acquired without tracking engaged [Figs. 4(f) and 5(f)]. Conversely, the coadded fundus images acquired with tracking engaged [Figs. 4(e) and 5(e)] retain almost all of the clarity of the retinal features of the single fundus image [Figs. 4(d) and 5(d)].

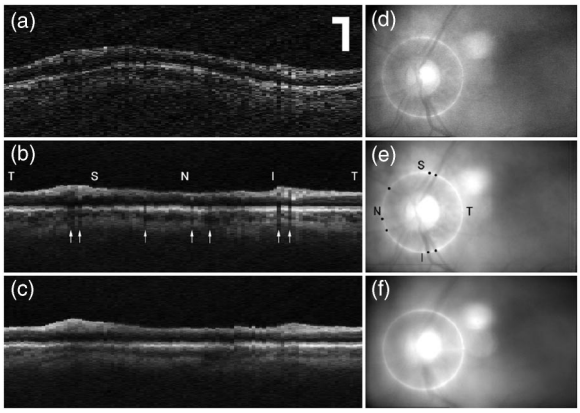

Fig. 4 Representative peripapillary scans for normal subject: (a) single OCT scan, (b) coadded OCT scan with tracking engaged, (c) coadded OCT scan with tracking disengaged, (d) fundus image corresponding to OCT scan in (a), (e) coadded fundus image corresponding to OCT image in (b), and (f) coadded fundus image corresponding to OCT image in (c). Scale bar for all images is 0.5 mm. (Normal subject 5, OS); T, temporal; S, superior; N, nasal; I, inferior.

5.2 *Disc Radial Scans*

For the peripapillary scans, a large number of consecutive images could be coadded and compared. For the radial scans (disc and macula), each set took several minutes and therefore only three each with and without tracking were acquired. The reduction of speckle and image improvement due to tracking is therefore less easily distinguishable in the three scan average. For this and other reasons, objective comparison of averaged images for the radial scans (disc and macula) was deferred. This analysis may eventually be performed to provide further characterization of any improvement that may be gleaned from the images.

Registration and edge analysis were applied to the disc radial scans as discussed in Secs. 4.2 and 4.3. Figure 6 shows representative averaged OCT and fundus images for a normal subject with and without tracking. The measured SNR for the coadded OCT images shown in Fig. 6 was 1.6 times greater than that for a single OCT image from the same set. Figure 7 plots the results of the edge detection algorithm. The motion is clear in Fig. 7(a). Also note the change in the shape of the

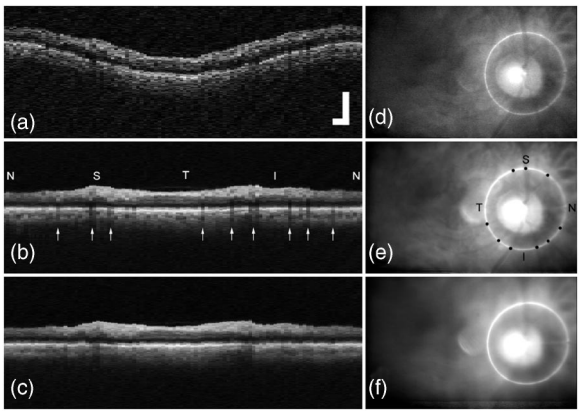

Fig. 5 Representative peripapillary scans for glaucoma subject. Images arranged as in Fig. 4. (Glaucoma subject 11, OD.)

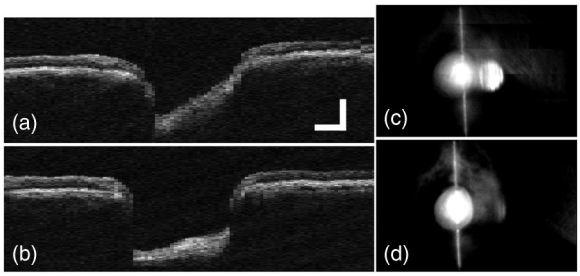

Fig. 6 Representative disc radial scan (1 of 6 in a set): (a) coadded OCT scan with tracking disengaged, (b) coadded OCT scan with tracking engaged, (c) coadded fundus image corresponding to OCT scan in (a), and (d) coadded fundus image corresponding to OCT scan in (b). (Glaucoma subject 5, OS.)

disc cup for run 3—the lack of the flat trough seen in the other profiles. This indicates an out-of-plane error, where large eye motion 90 deg to the direction of the OCT scan occurs.

Tables 2 and 3 list the results of the disc cup edge position analysis for normal and glaucoma subjects. The third and fourth columns refer to the mean variance (standard deviation) in edge position for all sets of all visits (both left and right edge) for the tracking (T) and nontracking (NT) trials. The standard deviation of each set of three scans was calculated, and then all scans (i.e., different radial angles) for all visits were averaged ($n=18$ for six radial angles and three visits, tracking or nontracking). The fifth column is the percentage of individual sets where the tracking standard deviation was less than the nontracking standard deviation. The sixth and seventh columns are the percentage of individual sets where the tracking standard deviation is less than a fixed threshold R of 2 pixels.

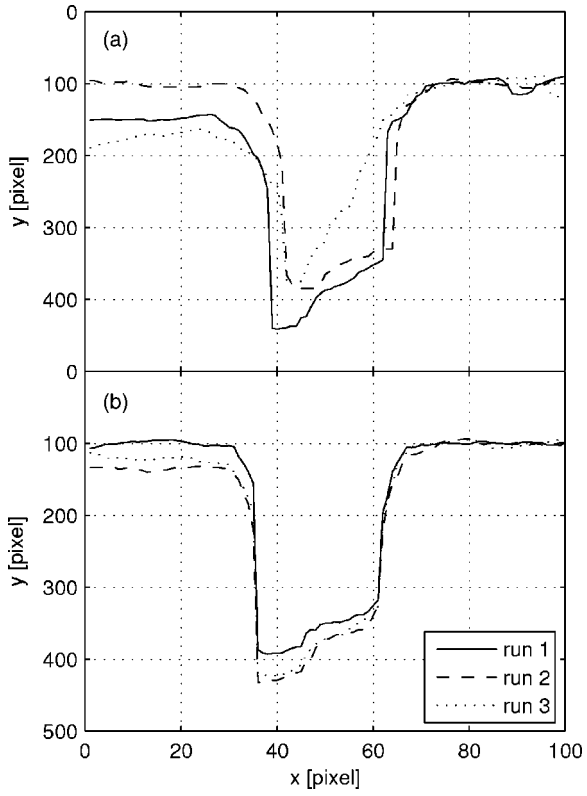

Fig. 7 Retinal edges for individual scans used to create images in Fig. 6: tracker (a) disengaged and (b) engaged.

Table 2 Disc edge statistics for normal subjects analyzed from individual visits (see text for a description).

Subject	Age	T_{avg} (pixel)	NT_{avg} (pixel)	$T<NT$ (%)	$T<R$[b] (%)	$NT<R$[b] (%)
1	26	0.98	1.46	0.50	0.89	0.69
2	47	1.32	3.25	0.75	0.81	0.44
3	33	0.50	1.65	0.81	1.00	0.72
4	39	0.65	2.05	0.81	0.94	0.58
5	34	0.50	1.87	0.92	1.00	0.75
6	50	0.85	1.52	0.78	0.94	0.64
7	58	0.70	2.13	0.88	1.00	0.63
8	34	0.64	2.27	0.92	0.97	0.39
9	50	0.74	2.37	1.00	1.00	0.45
10	54	0.63	1.48	0.79	1.00	0.79
11	39	0.63	2.58	0.94	1.00	0.44
Total	39[a]	0.76	2.07	0.82	0.95	0.59

[a] Median age.

[b] The threshold $R=2$ pixels.

5.3 *Macula Radial Scans*

Edge position analysis was also performed on the OCT scans collected from the foveal pit of each subject. However, since the signal is decreased in the fovea, the retinal edge is extremely difficult to measure regardless of the processing technique used. Therefore, a quantitative and automated analysis could not be completed for the macular scans because of the large number of software errors from retinal edge misidentification. Figures 8 and 9 show data collected on a glaucoma subject that had high enough brightness in the fovea to allow registration and measurement of retinal edge. The measured SNR for the coadded OCT images shown in Fig. 8 was 1.5 times greater than that for a single OCT image from the same set.

Table 3 Disc edge statistics for glaucoma subjects analyzed from individual visits.

Subject	Age	T_{avg} (pixel)	NT_{avg} (pixel)	$T<NT$ (%)	$T<R$ (%)	$NT<R$ (%)
1	42	0.81	2.24	0.83	0.97	0.56
2	74	1.12	1.78	0.81	0.81	0.61
3	85	1.82	3.2	0.77	0.66	0.31
4	70	1.03	3.24	0.64	0.92	0.25
5	57	0.51	2.00	0.96	0.96	0.58
6	77	0.96	1.71	0.75	0.92	0.67
7	68	1.04	2.07	0.82	0.85	0.58
8	55	1.07	1.74	0.71	0.86	0.67
9	70	1.91	2.48	0.67	0.78	0.47
10	75	1.17	2.54	0.79	0.85	0.39
11	63	0.75	1.66	0.81	0.92	0.69
Total	70	1.13	2.25	0.77	0.86	0.53

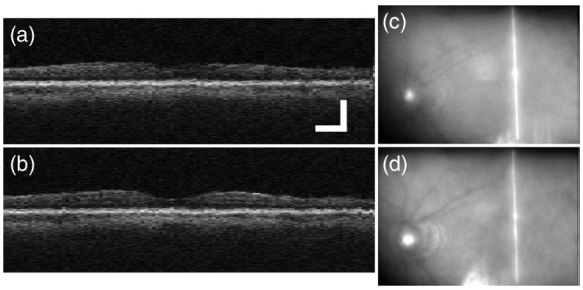

Fig. 8 Representative fovea radial scan. Images arranged as in Fig. 6. (Glaucoma subject 10, OS.)

5.4 *Comparison of Scans from Multiple Visits*

One of the significant improvements expected from TOCT is the ability to measure the same retinal location every time a patient is examined to monitor longitudinal progression of a disease or defect. To test the hypothesis that tracking improved the ability of the technician to return to a fixed retinal position, the variance in disc cup edge position for multiple visits was examined. For reasons related to platform integration, there were difficulties in comparing every visit of every subject that had nothing to do with tracking fidelity. The intervisit results for normal and glaucoma subjects are listed in Tables 4 and 5 and displayed in Fig. 10 for one normal subject. Tables 4 and 5 are arranged in a manner similar to Tables 2 and 3. However, the values in the third and fourth columns refer to the mean variance (standard deviation) in edge position calculated across visits. In other words, the standard deviation of nine scans was calculated and then all scans for each radial angle were averaged ($n=6$).

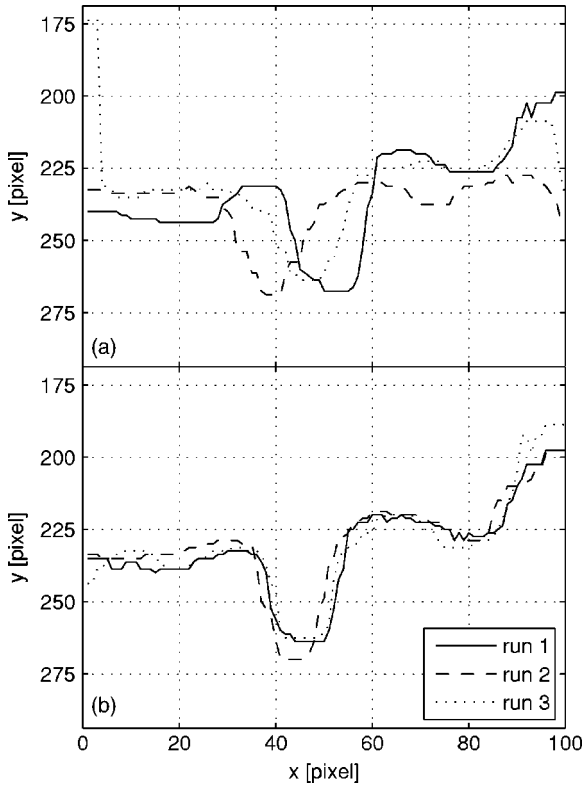

Fig. 9 Retinal edges for individual scans used to create images in Fig. 8: tracker (a) disengaged and (b) engaged.

Table 4 Disc edge statistics for normal subjects analyzed from multiple visits.

Subject	Number of Visits	T_{avg} (pixel)	NT_{avg} (pixel)	$T<NT$ (%)	$T<R$ (%)	$NT<R$ (%)
1	2	1.09	2.72	0.83	0.92	0.33
2	2	1.48	2.67	0.83	0.75	0.50
3	3	0.75	3.09	1.00	1.00	0.17
4	—	—	—	—	—	—
5	—	—	—	—	—	—
6	3	1.51	1.99	0.67	0.75	0.67
7	2	0.88	2.95	1.00	1.00	0.08
8	3	1.11	3.07	1.00	1.00	0.08
9	2	0.99	3.16	1.00	1.00	0.08
10	2	0.78	1.89	1.00	0.92	0.58
11	3	1.17	3.11	1.00	1.00	0.08
Total		1.08	2.74	0.93	0.93	0.29

6 Discussion

To summarize results, robust, continuous, repeatable, and clinically useful tracking on the lamina cribrosa was achieved in 96% of subjects tested in the clinical protocol. Examination of coadded peripapillary OCT images found an improvement in 100 and 94% of the images for normal and glaucoma subjects. Analysis of the mean variation in disc edge position found an improvement in every subject. The variation in individual sets found an improvement in 82 and 77% of intravisit sets and a reduction in standard deviation from greater than 2 (~120 μm) to approximately 1 pixel (~60 μm) for normal and glaucoma subjects. Similar analysis found an improvement in 93 and 94% of individual intervisit sets and a variance reduction from nearly 3 (~180 μm) to approximately 1 pixel (~60 μm) for normal and glaucoma subjects. Neither IOLs nor media opacities adversely affected tracking fidelity.

Table 5 Disc edge statistics for glaucoma subjects analyzed from multiple visits.

Subject	Number of Visits	T_{avg} (pixel)	NT_{avg} (pixel)	$T<NT$ (%)	$T<R$ (%)	$NT<R$ (%)
1	2	0.68	2.13	0.92	1.00	0.58
2	—	—	—	—	—	—
3	—	—	—	—	—	—
4	3	1.66	4.27	1.00	0.67	0.00
5	2	0.83	2.23	1.00	1.00	0.33
6	3	1.29	2.79	1.00	1.00	0.00
7	—	—	—	—	—	—
8	2	1.18	2.85	0.92	0.83	0.33
9	3	2.83	3.31	0.67	0.33	0.08
10	2	0.95	3.29	1.00	0.92	0.00
11	3	0.95	2.32	1.00	0.92	0.33
Total		1.30	2.90	0.94	0.83	0.21

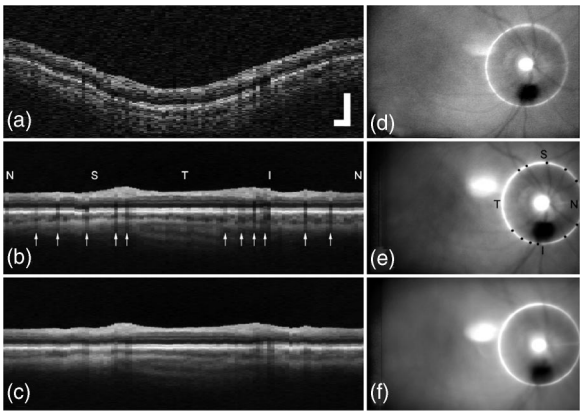

Fig. 10 Representative OCT scans for multiple visits: (a) single OCT scan from one visit, (b) coadded OCT scan combined from three visits with tracker engaged, (c) coadded OCT scan combined from three visits with tracker disengaged, (d) fundus image corresponding to OCT scan in (a), (e) coadded fundus image corresponding to OCT image in (b), and (f) coadded fundus image corresponding to OCT image in (c). (Normal subject 3, OD.)

As already noted, the purpose of the peripapillary scans is to measure RNFL thickness for early diagnosis of glaucoma. Although preliminary analysis of RNFL thickness found no improvement due to tracking,[12] RNFL thickness may not be an appropriate measurement endpoint for the characterization of improvement due to tracking. This is because the effect of tracking may not be revealed within the typical RNFL standard deviation ($\leqslant 10$ μm with ~ 120-μm mean). As seen in Figs. 4 and 5, the shallow gradients of these layers render such measures less sensitive to transverse motion. This does not mean that tracking is not effective in obtaining more accurate RNFL metrics, and therefore potentially more sensitive and specific glaucoma diagnosis. Rather it means that an improvement should be made in the methodology of standard clinical RNFL measurements. For example, in other current (e.g., Stratus OCT) and future systems, there is an improvement in both transverse and axial image resolution. The improved resolution should inevitably yield higher precision values for RNFL thickness. Also, as illustrated by Figs. 4 and 5, an increase in the number of coadded OCT images will significantly reduce speckle artifacts. A 5% change in RNFL is significant loss. Without tracking, the effect of motion is masked by co-adding noisy scans. This constraint no longer exists with TOCT: boundaries will become better defined only by averaging because high image spatial frequencies are preserved with tracking.

In Figs. 4 and 5, the overall appearance of the averaged peripapillary scans with and without tracking is similar because the layer thickness does not change rapidly in the retinal plane. However, with tracking the most significant improvement is in resolving fine structure. Shadows of major retina vessels and often the vessels themselves can be clearly seen. Note that considerably greater structure in the underlying choroidal vessels is also evident. Further, there is a subtle enhancement of the contrast at the outer boundary of the RNFL. These features are easily understood because tracking causes successive images to align in the transverse directions to much better precision than the ~ 110-μm pixel size. The positions of fine scale features never shift. Further, compensation of transverse motion will enhance the performance of the vertical alignment algorithm providing a better estimation of true retinal profile.

Since only three radial scans (disc cup and macula) at any angle were collected and coadded, the reduction of speckle is not as dramatic in Figs. 6 and 8. In Fig. 6(a), the true shape of the cup is distorted because of out-of-plane motion (see later). The disc cup edge in Figs. 6(a) and 6(c) is broadened and blurred compared to Figs. 6(b) and 6(d). Without tracking, vertical alignment suffers somewhat from motion—tending to make boundaries visibly fuzzier. In Fig. 8(a), the foveal pit is not visible and the retinal boundary in this region blurred. Retinal layers visible on either side of the fovea (more clearly to the right) with tracking [Fig. 8(b)] are completely washed out in the nontracking case [Fig. 8(a)]. Tracking thus provides a benefit by making low contrast boundary detection more robust. But this benefit may not be resolvable with only three scans. The effect lies within the standard deviation of the image noise statistics for so few scans, at least for good fixators. Figure 9 also illustrates one reason why extraction of edge and area information from the foveal pit is more difficult than that for the disc cup: because the pit area is much smaller and the edges more shallow (note the $5\times$ reduction in scale of Fig. 9 compared to Fig. 7). The other primary reason is that the OCT signal is reduced in the foveal pit because of the absence of overlying layers that are more highly scattering and thus produce a clear demarcation of retinal edge.

The appearance of OCT images coadded from three visits in Fig. 10 is similar to the images coadded from single visits in Figs. 4 and 5. Since this subject (normal subject 3) was a fairly good fixator and for the reasons discussed above, the appearance of some layers is preserved in the nontracking coadded OCT image [Fig. 10(c)]. However, distinct layers of both the retina and choroid are blurred in the nontracking OCT image where they are clear and sharp in the tracking OCT image [Fig. 10(b)]. Moreover, the location of blood vessels, denoted by their shadows, are preserved and enhanced in comparison to the single scan [Fig. 10(a)]. The effect of tracking as illustrated by the fundus images [Figs. 10(d) to 10(f)] is clear.

Before a full discussion of the quantitative analysis presented in Tables 2 to 5, one consideration of the method of data analysis alluded to in Sec. 4.3 must be fully explained. For many of the nontracking scans, eye motion with a large vector component normal to the OCT scan was large enough to prohibit measurement of disc cup edge position. This large out-of-plane motion is illustrated in Fig. 11. In Figs. 11(a) and 11(d), an appropriate scan through the center of the disc is made. In the very next scan, Figs. 11(b) and 11(e), the motion was large enough so that no portion of the disc was scanned. Figures 11(c) and 11(f) show the coadded OCT and fundus images from this set. Obviously, the edge position of the disc cup cannot be measured for this large motion. Therefore, the entire set was thrown out. The effect of this is to make the standard deviation in Tables 2 to 5 for the nontracking cases artificially lower than is actually the case. Mild out-of-plane motion is also illustrated in the retinal edge position in run 3 of Fig. 7(a).

It is clear from the results of the disc cup edge analysis presented in Tables 2 and 3, that there was a wide range of

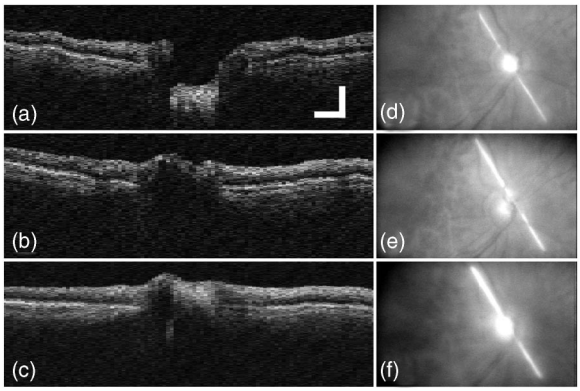

Fig. 11 Large out-of-plane motion, common only in the nontracking case, made coaddition of images and measurement of disc cup edge impossible: (a) single OCT scan centered on disc, (b) single OCT scan with large position error, (c) coadded OCT image from three individual scans including (a) and (b), (d) single fundus image corresponding to OCT scan in (a), (e) single fundus image corresponding to OCT scan in (b), and (f) coadded fundus image corresponding to OCT scan in (c). (Glaucoma subject 1, OD.)

fixators in both the normal and glaucoma groups. This can be seen in the ''NT avg'' column, which displays the variation in disc cup edge under normal, non-tracking conditions. It should be emphasized that the standard deviation calculation made in these tables is a measure of the variance and is different from the peak-to-peak amplitude of eye motion estimated in Sec. 4 to be 0.5 deg ($\sim$150 μm) or 2.5 pixels for radial scans for a good fixator. The peak-to-peak amplitude can be several (i.e., 2 to 4) times larger than the standard deviation. Thus, a range from 1.46 to 3.25 for normal subjects and 1.66 to 3.24 for glaucoma subjects for the standard deviation means a wide range of fixators were present in the sample, with the normal subjects slightly better fixators overall.

Although the overall standard deviation (i.e., mean for all sets) was reduced for all subjects when tracking was engaged, an improvement was found in only 82 and 77% of individual sets for normal and glaucoma subjects, respectively. Further examination of the data shows that the normal subjects that had particularly low percentages were generally the best fixators (Table 2). For example, the three best fixators (subjects 1, 10, and 6) had three of the four worst percentages. This leads to the obvious conclusion that tracking will be less useful for good fixators, subject to the transverse image resolution. That is, if the amplitude of involuntary eye motion in a subject is lower than the pixel resolution of the imaging technique, then tracking can improve position accuracy only to the size of an individual pixel. In current and future high-bandwidth OCT systems, the limiting factor may be tracking accuracy rather than transverse pixel resolution. For example, the current CZMI Stratus OCT system uses 500 transverse pixels, or an improvement of fivefold in resolution to $\sim$12 μm, near the tracking accuracy found in other systems [$<$15 μm for TSLO (Ref. 9)].

The limiting factor of transverse pixel resolution on tracking performance can also be seen in the overall reduction in standard deviation from tracking to nontracking. While the nontracking standard deviation in disc cup edge position is correlated to the physiological factors that determine involuntary eye motion amplitude, the tracking standard deviation is limited by the image resolution. We expect that as the transverse pixel resolution is decreased to the limit of tracking accuracy, the variation in edge position will remain between 0.5 and 1 pixel for most subjects with tracking engaged, but will increase to the pixel equivalent for the range of fixators tested without tracking engaged (from approximately 0.5 deg or 150 μm for the best fixators).

Although there is a slight difference in disc cup edge position standard deviation between normal and glaucoma subjects, the degree to which this difference is significant is not known. Most of the problems may be traced to factors unrelated to tracking. For example, some glaucoma subjects had intraocular lenses (IOLs) that caused a drastic degradation of the OCT signal. Although this did not affect tracking robustness, it made extraction of information from poor OCT images difficult. There was also an increase in other problems with the glaucoma group that were not related to the performance of the TOCT system (e.g., subject attentiveness, etc.). As mentioned previously, there were also several subjects in the glaucoma group that had multiple tracking points within the optic nerve disc. These patients require particular attention from the operator. Many of these problems are inevitable in a clinical environment. It is expected that in clinical testing with higher resolution OCT instruments, the tracker would give transverse scan alignment absolutely equivalent to the normal subjects—better than is possible for even the highest functioning fixators. It is under such circumstances that the clinical value of TOCT will be most evident.

When the data are resorted to compare disc cup edge variance between visits (Tables 4 and 5), it is clear that tracking improves the registration of OCT images from visit to visit. An improvement in overall standard deviation was again seen in all subjects, with improvement in 93 and 94% of individual sets. This increased improvement results from the capability of the tracking system to continually return the OCT imaging beam to the same pixel coordinates. Conversely, without tracking, the operator is relied upon to locate the same disc cup position from the fundus image. (For macular scans, this degradation from visit to visit may not be as profound because the OCT scan automatically goes through the center of the fixation point, that is, the fovea.) Thus, between visits with tracking engaged, the disc cup edge position variation is less than a fixed threshold (2 pixels) the same percentage of time as within visits (see ''$T<R$'' columns in Tables 2 to 5). However, for the same fixed threshold with no tracking, the percentage drops between visits compared to within visits (''NT$<R$'' columns in Tables 4 and 5 compared to 2 and 3). This is also seen in the large increase from approximately 2 to 3 in the total nontracking standard deviation. The slight increase in tracking standard deviation probably results from the accuracy of a calibration method ($\pm$1 pixel), which was required to align coordinate axes of the OCT and tracker components of the TOCT. If tracking were fully integrated with OCT scanning, we would expect the tracking standard deviation to be identical within and between visits.

Recently, a technology called spectral domain OCT (SDOCT) has been introduced for very high speed acquisition of OCT images. SDOCT uses a spectrometer and linear array in the detector path rather than the traditional photodiode de-

tector. By taking the Fourier transform of the linear array output, light is simultaneously collected from all range gates that make up the A scan within the focal volume. This can be done with improved SNR because SDOCT has an inherent multiplexed advantage.[13] SDOCT can therefore acquire A scans at the line rate of the linear array, up to tens of kilohertz. This translates to frame rates exceeding 100 frames/s for a well-sampled transverse section. The speed of SDOCT makes individual transverse sections less susceptible to eye motion artifacts. However, SDOCT imaging will still benefit from retinal tracking for several important applications. First, even moderately sampled 3-D maps made up of multiple transverse sections will require several seconds in the fastest SDOCT systems. These maps may be difficult to construct without some means of stabilization, and the full potential of SDOCT may thus go unrealized. Second, retinal tracking improves the ability to align the scan to the same retinal coordinates for longitudinal studies to track disease progression. Although postprocessing techniques can be used to align individual scans to retinal landmarks with accuracy dependent on the fundus imaging technique, relocation to those coordinates for subsequent scans would still be subject to fixational precision. Third, as shown in this paper, retinal tracking enables a reduction in noise and speckle by coadding large numbers of transverse scans.

For this laboratory TOCT instrument, these results show a clear and significant enhancement of scan position accuracy and reproducibility for retinal tracking compared to fixation. Fine structure not readily resolved in single scans can easily be seen in averaged images. In the coadded images acquired without tracking, the finest scales are washed out—typically over three or more image pixels (over 300 μm microns at 110 μm/pixel, i.e., motion of $\sim$1 deg). This motion occurs both laterally, and most problematically, in and out of the image plane. This blurring and distortion is particularly clear with scans through the disc with steep vertical features, at the fovea, and with circular scans with blood vessel and their shadows. The precise shape of cup, disc, and rim area may be degraded when this effect is large. In multiframe averages of circular scans around the disc, disc radial scans, and macular scans, the reduction in speckle is significant, while the fine structure is still clear. The vessel shadows line up perfectly in all tracked images taken over the hour-long visit duration in all subjects, boundaries are sharp, choroidal vessel structure is evident. For nearly all subjects, the effect of tracking is to make everyone a perfect fixator, regardless of age and eye motion characteristics. The observed level of transverse scan reproducibility appears to be consistent with the requirements for potential acquisition of high-quality, long-duration complex scan patterns (e.g., 3-D maps).

Acknowledgments

This work was funded by the National Institutes of Health (National Eye Institute) under grants EY13036 and EY13178. Both Physical Sciences Inc. (PSI) and Carl Zeiss Meditec Inc. (CZMI) provided partial support for the clinical tests.

References

1. C. A. Puliafito, M. R. Hee, J. S. Schuman, and J. G. Fujimoto, Eds., *Optical Coherence Tomography of Ocular Diseases*, Slack Inc., Thorofane, NJ (1996).
2. P. Massin, G. Duguid, A. Erginay, B. Haouchine, and A. Gaudric, ''Optical coherence tomography for evaluating diabetic macular edema before and after vitrectomy,'' *Am. J. Ophthalmol.* **135**, 169–177 (2003).
3. Y. Ikuno, K. Sayanagi, T. Oshima, F. Gomi, S. Kusaka, M. Kamei, M. Ohji, T. Fujikado, and Y. Tano, ''Optical coherence tomographic findings of macular holes and retinal detachment after vitrectomy in highly myopic eyes,'' *Am. J. Ophthalmol.* **136**, 477–481 (2003).
4. R. F. Spaide, J. K. Lee, J. K. Klancnik, and N. E. Gross, ''Optical coherence tomography of branch retinal vein occlusion,'' *Retina* **23**, 343–347 (2003).
5. C. Bowd, L. M. Zangwill, C. C. Berry, E. Z. Blumenthal, C. Vasile, C. Sanchez-Galeana, C. F. Bosworth, P. A. Sample, and R. N. Weinreb, ''Detecting early glaucoma by assessment of retinal nerve fiber layer thickness and visual function,'' *Invest. Ophthalmol. Visual Sci.* **42**, 1993–2003 (2001).
6. V. Guedes, J. S. Schuman, E. Hertzmark, A. Correnti, R. Mancini, G. Wollstein, D. Lederer, S. Voskanian, L. Velazquez, H. M. Pakter, T. Pedut Kloizman, J. G. Fujimoto, and C. Mattox, ''Optical coherence tomography measurement of macular and nerve fiber layer thickness in normal and glaucomatous human eyes,'' *Ophthalmology* **110**, 177–189 (2003).
7. A. M. Rollins, M. D. Kulkarni, S. Yazdanfar, R. Ungarunyawee, and J. A. Izatt, ''In vivo video rate optical coherence tomography,'' *Opt. Express* **3**, 219–229 (1998); http://www.opticsexpress.org/abstract.cfm?URI=OPEX-3-6-219.
8. R. D. Ferguson, ''Servo tracking system utilizing phase-sensitive detection of reflectance variation,'' U.S. Patents No. 5,767,941 (1998) and No. 5,943,115 (1999).
9. D. X. Hammer, R. D. Ferguson, J. C. Magill, M. A. White, A. E. Elsner, and R. H. Webb, ''Compact scanning laser ophthalmoscope with high speed retinal tracker,'' *Appl. Opt.* **42**, 4621–4632 (2003).
10. D. X. Hammer, R. D. Ferguson, J. C. Magill, M. A. White, A. E. Elsner, and R. H. Webb, ''Image stabilization for scanning laser ophthalmoscopy,'' *Opt. Express* **10**, 1542–1549 (2002); http://www.opticsexpress.org/abstract.cfm?URI=OPEX-10-26-1542.
11. D. X. Hammer, R. D. Ferguson, J. C. Magill, M. A. White, A. E. Elsner, and R. H. Webb, ''Tracking scanning laser ophthalmoscopy (TSLO),'' in *Ophthalmic Technologies XIII*, F. Manns, P. G. Söderberg, and A. Ho, Eds., *Proc. SPIE* **4951**, 208–217 (2003).
12. S. Beaton, H. Ishikawa, G. Wollstein, D. M. Stein, R. D. Ferguson, D. X. Hammer, and J. S. Schuman, ''Nerve fiber layer (NFL) thickness measurement with tracking OCT,'' in *Proc. Annu. Meeting of Association of Research in Vision and Ophthalmology (ARVO)*, Abs. 5508 (2004).
13. J. F. de Boer, B. Cense, B. H. Park, M. C. Pierce, G. J. Tearney, and B. E. Bouma, ''Improved signal-to-noise ratio in spectral-domain compared with time-domain optical coherence tomography,'' *Opt. Lett.* **28**, 2067–2069 (2003).